Article

Not peer-reviewed version

Fucoidan and Hyaluronic Acid Modified ZE21B Magnesium Alloy for Potential Application as Cardiovascular Stents

Haoran Wang , Yunwei Gu , Qi Wang , Lingchuang Bai * , Shaokang Guan

Posted Date: 13 May 2025

doi: 10.20944/preprints202505.0925.v1

Keywords: magnesium alloy; vascular stent; surface modification; corrosion resistance; biocompatibility

 doi:10.20944/preprints202505.0925.v1

Article

Fucoidan and Hyaluronic Acid Modified ZE21B Magnesium Alloy for Potential Application as Cardiovascular Stents

Haoran Wang [1], Yunwei Gu [1,2], Qi Wang [1,2], Lingchuang Bai [1,2,*] and Shaokang Guan [1,2,3]

[1] School of Material Science and Engineering, Zhengzhou University, Zhengzhou, 450001, 100 Science Road, P. R. China

[2] Henan Key Laboratory of Advanced Light Alloy, Zhengzhou, 450001, 100 Science Road, P. R. China

[3] Key Laboratory of Materials Processing and Mold Technology (Ministry of Education), Zhengzhou 450001, 100 Science Road, P. R. China

* Correspondence: lcbai@zzu.edu.cn

Abstract: Magnesium alloy stents have great potential for the treatment of cardiovascular and cerebrovascular diseases due to their excellent mechanical supportability and biodegradability. However, bare magnesium alloy stents often degrade too rapidly and demonstrate insufficient biocompatibility, severely limiting their clinical applicability. Herein, a composite coating consisting of MgF_2 conversion layer, polydopamine (PDA) layer, fucoidan, and hyaluronic acid was prepared to enhance the corrosion resistance and biocompatibility of ZE21B alloy for vascular stent application. The modified ZE21B alloy exhibited relatively high surface roughness, moderate wettability, and better corrosion resistance. Moreover, the modified ZE21B alloy with low hemolysis rate and fibrinogen adsorption level confirmed improved hemocompatibility for medical requirements. Furthermore, the ZE21B alloy modified with fucoidan and hyaluronic acid could promote the adhesion, proliferation, and NO release of ECs, and meanwhile inhibit the adhesion and proliferation of SMCs and promote the competitive growth of ECs over SMCs due to the synergistic effect of natural fucoidan and hyaluronic acid. The modification with fucoidan and hyaluronic acid significantly enhanced the corrosion resistance and biocompatibility of ZE21B magnesium alloy, thereby providing a simple and effective strategies for the development of biodegradable vascular stents.

Keywords: magnesium alloy; vascular stent; surface modification; corrosion resistance; biocompatibility

1. Introduction

The global prevalence of cardiovascular disease is alarming, as it continues to be one of the leading causes of mortality worldwide. Interventional therapies, such as percutaneous coronary interventions, can rapidly alleviate blockages in blood vessels by restoring blood flow through balloon dilation and stent placement [1]. Traditional non-degradable vascular stents, including 316L stainless steel, nickel-titanium alloy, and cobalt-based alloy, can elicit local inflammatory responses when retained in the body for extended periods [2]. These responses may stimulate the proliferation of vascular smooth muscle cells (SMCs), contribute to intimal hyperplasia, and ultimately result in in-stent restenosis. Magnesium alloy vascular stents have excellent biodegradability and mechanical support properties, which can overcome the many shortcomings of traditional non-degradable stents and have great potential in the field of cardiovascular disease intervention [3,4]. However, magnesium alloys degrade at an excessive rate and do not possess the necessary biological functions to fulfill the clinical requirements for vascular stents. Consequently, employing various surface modification techniques to enhance the corrosion resistance and biological functionality of

 doi:10.20944/preprints202505.0925.v1

magnesium alloys represents an effective strategy for addressing the current challenges associated with magnesium alloy stents [5–7].

Currently, a variety of methods are available to enhance the corrosion resistance of magnesium alloys. One approach involves modifying the alloy composition by adding elements such as aluminum and rare earths to refine the grain structure and reduce impurities, thereby promoting element homogenization and improving corrosion resistance [8]. Another strategy is the application of surface protection treatments [9], including chemical conversion processes to create protective passive films [10], and micro-arc oxidation to produce a controllable thickness of a ceramic layer that offers the resistance to both corrosion and wear [11]. The magnesium fluoride (MgF_2) layer serves a crucial function as a chemical conversion coating, significantly enhancing the corrosion resistance of magnesium alloys [12,13]. The chemical reaction between magnesium alloy and hydrofluoric acid solution results in the formation of a MgF_2 layer. This MgF_2 layer is insoluble in water, allowing it to adhere easily to the surface of the magnesium alloy and create a smooth, dense film. The MgF_2 layer effectively prevents corrosive media from contacting the magnesium substrate, thereby reducing the corrosion rate. In corrosive environments, such as bodily fluids, the MgF_2 layer significantly enhances the corrosion resistance of magnesium alloy.

Magnesium alloy stents should have excellent biocompatibility in addition to appropriate corrosion resistance. The MgF_2 layer can significantly enhance the corrosion resistance of magnesium alloys; however, it lacks the biological functionality necessary for vascular stents. Polydopamine (PDA) coatings exhibit excellent biocompatibility and low cytotoxicity, characterized by their strong adhesion capabilities, allowing them to adhere firmly to a variety of substrates [14–16]. Furthermore, PDA coatings are rich in functional groups and facilitate convenient secondary functional modifications. The application of PDA coating to the surface of magnesium alloy stents not only protects the magnesium alloy from rapid degradation but also acts as an intermediate layer, offering reactive sites for subsequent modifications of the magnesium alloy. As a naturally occurring marine polysaccharide, fucoidan exhibits a range of biological functions, including anticoagulant, antithrombotic, and anti-inflammatory properties [17]. Additionally, it modulates vascular cell behavior, enhances endothelial cell (EC) adhesion and proliferation on vascular scaffolds, and decreases the risk of restenosis [18,19]. Hyaluronic acid serves as a crucial component of the vascular extracellular matrix and significantly influences vascular cell behavior, including promoting cell adhesion, proliferation, migration, and differentiation [20,21]. Additionally, hyaluronic acid enhances angiogenesis, emulates natural mechanisms, creates a supportive microenvironment for EC growth, diminishes platelet activation and adsorption capacity, and facilitates vascular endothelialization [23,24]. Therefore, it was expected that a composite coating consisting of MgF_2 layer, polydopamine (PDA) layer, fucoidan, and hyaluronic acid could significantly enhance the corrosion resistance and biocompatibility of Mg-Zn-Y-Nd (ZE21B) magnesium alloy for vascular stent application.

In this work, a composite coating consisting of MgF_2 layer, PDA layer, fucoidan, and hyaluronic acid was constructed on ZE21B magnesium alloy to enhance the corrosion resistance and biocompatibility for vascular stent application. Briefly, ZE21B magnesium alloy was first passivated with hydrofluoric acid to form a dense and homogeneous MgF_2 layer, and then deposited in dopamine hydrochloride solution to obtain a PDA coating, followed by the immobilization of natural fucoidan and hyaluronic acid. The surface micromorphology, surface chemical component and chemical structure, surface wettability, and corrosion resistance of the ZE21B alloy modified with the fucoidan and hyaluronic acid were characterized. The hemolysis assays and fibrinogen adsorption assays were conducted to evaluate the hemocompatibility of the modified ZE21B alloy. The adhesion, proliferation, and NO release of ECs, the adhesion, and proliferation of SMCs, and the competitive growth behavior of ECs and SMCs in a coculture experiment were systematically investigated to assess the cytocompatibility of the modified ZE21B alloy.

 doi:10.20944/preprints202505.0925.v1

2. Materials and Methods

2.1. Materials

Mg-Zn-Y-Nd alloy (ZE21B, 2.00wt% Zn, 0.46wt% Y, 0.50wt% Nd) was self-developed by Henan Key Laboratory of Advanced Light Alloy (Zhengzhou, China). Hydrofluoric acid (HF) was bought from Haohua Chemical Reagent Co., Ltd. (Luoyang, China). Dopamine (DA) hydrochloride was purchased from Beijing HWRK Chemical Technology Co. Fucoidan and hyaluronic acid were purchased from Shanghai Macklin Biochemical Technology Co., Ltd. Human umbilical artery smooth muscle cells (SMCs) and venous endothelial cells (ECs) were provided by the Shanghai Cell Bank, Chinese Academy of Sciences. Nitric oxide (NO) assay kit and cell counting kit-8 (CCK-8) were obtained by Shanghai Biyuntian Biotechnology Co. FITC-phalloidin and DAPI and TMB were purchased from Solarbio Biotechnology Co., Ltd. (Beijing, China). An anti-human fibrinogen-HRP Conjugated antibody produced in goat was purchased from Beijing Solepol Co. Anti-human fibrinogen γ-chain antibody was purchased from Shanghai Huzheng Biotechnology Co.

2.2. Preparation of Fucoidan and Hyaluronic Acid Modified ZE21B Alloy

Magnesium alloy (ZE21B) samples (10 mm in diameter, 3 mm in thickness) was polished with progressively finer sandpapers (200#, 400#, 600#, 800#, and 1000#) to obtain the optimal surface quality. After drying, these as-prepared samples were labeled as ZE21B. Subsequently, the polished ZE21B samples were immersed in a 40% (v/v) HF solution for 48 h at ambient temperature to form a uniform MgF_2 protective coating, with the resulting samples labeled as ZF. These fluoridated samples were then rinsed copiously with deionized water and dried for further use. The ZF samples were deposited in DA solution (2 mg/mL, pH = 8.5) at room temperature for 24 h to produce the polydopamine (PDA) coating for further immobilization of fucoidan and hyaluronic acid. The PDA deposited samples were then incubated in the mixed solution at 30°C for 4 h, with fixed fucoidan concentration (0.5 mg/mL) and varying hyaluronic acid concentration (1.0 mg/mL, 3.0 mg/mL, and 5.0 mg/mL), and the corresponding samples were denoted as ZFFHI, ZFFHII, and ZFFHIII, respectively.

2.3. Characterization of Fucoidan and Hyaluronic Acid Modified ZE21B Alloy

The surface micromorphology of unmodified and modified ZE21B alloy samples was observed by scanning electron microscope (SEM, ZEISS Sigma 360, Germany) at an accelerating voltage of 5 kV. The surface chemical composition of the samples was analyzed by X-ray photoelectron spectrometer (XPS, Thermo ESCALAB 250XI, UK) operating at 5×10^{-10} Torr with Al Kα as the radiation source. The surface chemical structure of the samples was detected by attenuated total reflection Fourier transform infrared spectroscopy (ATR-FTIR, Nicolet iS 10, USA) over a range of 4000 ~ 600 cm^{-1} through 32 scans. The surface wettability of the samples was measured using an easy-drop goniometer (Powereach JC2000C). The droplet volume was set as 3 μL, and the average water contact angle value was calculated from five repeat measurements. The corrosion resistance of the samples in Hanks' solution was studied by a three-electrode electrochemical system (Risetest RST5200F, China). The auxiliary electrode was the platinum electrode, the reference electrode was the saturated calomel electrode (SCE), and the working electrode was the sample. The kinetic potential polarization curves were displayed at a scan rate of 0.001 V/s in the range of -2.0 V ~ -1.0 V (vs. SCE). The corrosion potential and corrosion current density was fitted based on the polarization curves detected for the three electrochemical systems.

2.4. Hemolysis Rate of Fucoidan and Hyaluronic Acid Modified ZE21B Alloy

Hemolysis assay was conducted to evaluate the hemocompatibility of the ZE21B alloy modified with fucoidan and hyaluronic acid. Physiological saline was used as the negative control group, and ultrapure water was used as the positive control group. Fresh human whole blood was collected from

 doi:10.20944/preprints202505.0925.v1

healthy volunteers and diluted with physiological saline at a ratio of 4 : 5. First, ZE21B, ZF, ZFFHI, ZFFHII, and ZFFHIII samples were placed into separate 15 mL centrifuge tubes, with 10 mL of physiological saline added to each tube. For the control groups, 10 mL of physiological saline and ultrapure water were added, respectively. All tubes were then placed in a water bath at 37°C for 30 min. Subsequently, 200 μL of the diluted blood was added to each tube, and the tubes were incubated in the 37°C water bath for 1 h. After incubation, 6 mL from each tube was transferred to a new centrifuge tube, and the samples were centrifuged at 2500 rpm for 15 min. Finally, 100 μL of the supernatant from each sample was transferred to a 96-well plate, and the absorbance at 540 nm was measured using a microplate reader. The hemolysis rate was calculated using the following formula:

$$\text{Hemolysis rate } (\%) = \frac{OD_t - OD_n}{OD_p - OD_n} \times 100\% \quad (1)$$

OD_t, OD_n, and OD_p are the absorbance values of the experimental group, negative control group, and positive control group, respectively.

2.5. Fibrinogen Adsorption of Fucoidan and Hyaluronic Acid Modified ZE21B Alloy

Platelet-poor plasma (PPP) was obtained by centrifuging fresh blood collected from healthy volunteers at 3000 rpm for 15 min. Subsequently, 80 μL of PPP was added to the surfaces of the ZE21B, ZF, ZFFHI, ZFFHII, and ZFFHIII samples, which were incubated at 37°C for 1 h. After washing with physiological saline, 50 μL of 5% bovine serum albumin (BSA) blocking solution was added to the sample surfaces and incubated at 37°C for 0.5 h. The samples were then washed again with physiological saline. 20 μL HRP-conjugated goat anti-human fibrinogen adsorption antibody solution (antibody: saline = 1:500, v/v) was added to the sample surfaces and incubated at 37°C for 1 h. After washing and removing any residual liquid, 100 μL tetramethylbenzidine (TMB) solution were added onto the sample surfaces and kept in the dark for 10 min. Finally, 50 μL H_2SO_4 solution was added to stop the chromogenic reaction. The absorbance of final solution was measured at 450 nm by a microplate reader.

2.6. Growth Behavior of ECs and SMCs on ZE21B Alloy Modified with Fucoidan and Hyaluronic Acid

The ECs were cultured on ZE21B, ZF, ZFPCI, ZFPCII, and ZFPCIII samples at a density of 1.0×10^4 cells/mL to investigate the growth behavior. At the predetermined time points (1 day and 3 days), the samples were removed to a new 24-well plate, washed with PBS and fixed in 4% paraformaldehyde solution for 30 min. After that, the samples were treated with 0.5% Triton X-100 solution for 5 min, and sealed with 5% BSA solution for 30 min. Then, ECs on the samples were stained with 5 μL/mL FITC-labeled phalloidin and 5 μL/mL DAPI in the dark for 50 min and 4 min, respectively. Finally, the fluorescence images of ECs on each sample were recorded using a multifunctional confocal laser scanning microscope (CLSM, Nikon C2 Plus, Japan).

To determine the proliferation of ECs on the samples, the Cell Counting Kit-8 (CCK-8) assay was performed at the predetermined time points (1 day and 3 days). The cell culture procedure was the same as above. At day 1 and day 3, CCK-8 solution was added to the 24-well culture plates and incubated continuously for 3 h. Then, 100 μL of the solution was transferred into a 96-well plate and the absorbance of each well was measured at 450 nm using an enzyme meter.

The NO release from ECs on the samples was determined by the NO detection kit. ECs were seeded onto the samples at a density of 1.0×10^4 cells/mL. After 1 day and 3 days, 50 μL of supernatant from each well was collected into the 96-well plate. Subsequently, 50 μL Griess I and 50 μL Griess II solutions were added into the 96-well plate, respectively. Finally, the absorbance of the mixed solution was measured at 540 nm using an enzyme meter.

The growth behavior of SMCs on the samples were also investigated through the cell fluorescence staining assay and CCK-8 assay. The seeding density of SMCs on the samples was of 8.0×10^3 cells/mL, and the other culture and experimental procedures of SMCs on the samples were similar to those of ECs.

 doi:10.20944/preprints202505.0925.v1

2.7. Coculture of ECs and SMCs on ZE21B Alloy Modified with Fucoidan and Hyaluronic Acid

The competitive growth of SMCs and ECs on the samples were evaluated through the coculture experiment. ECs and SMCs were stained with green and red by CMFDA and CFDA fluorescent probes, correspondingly. The same number of ECs and SMCs were seeded onto the sample surface at 5×10^3 cells per well. After 24 h of culture, the samples were fixed in 4% paraformaldehyde solution for 30 min and rinsed three times with PBS solution. Then the fluorescence images of ECs and SMCs on the samples were recorded by CLSM. The cell densities of ECs and SMCs as well as the ECs/SMCs ratios were also calculated from the fluorescence images of ECs and SMCs.

2.8. Statistical Analysis

The data used for all statistical analysis were obtained from at least three independent experiments and are expressed as the mean ± standard deviation. Significance analysis was performed using one-way analysis of variance (ANOVA), with $^*P<0.05$ indicating that the differences between the data were statistically significant.

3. Results and Discussion

3.1. Characterization of Fucoidan and Hyaluronic Acid Modified ZE21B Alloy

The SEM images of ZE21B, ZF, ZFFHI, ZFFHII, and ZFFHIII samples at different magnifications (3000 × and 10000 ×) were shown in Figure 1a. The ZE21B sample exhibited a flat and smooth surface at both low and high magnification, except for the presence of some scratches due to the polishing processes. After fluoridation, the surface of ZF sample was smooth and flat without obvious defects at low magnification, while a large number of fine particulate matter and a small number of holes appeared on the surface of ZF sample at high magnification. The fine particulate matter may have been formed by the MgF_2, while the holes may have resulted from the leaching of second-phase precipitates from the ZE21B alloy during the fluoridation reaction. After the deposition of PDA and the immobilization of fucoidan and hyaluronic acid, many micro-/nano-particles appeared the surfaces of ZFFHI, ZFFHII, and ZFFHIII samples under the observation at low magnification, and the roughness of these sample surfaces became larger compared with that of ZF sample. Under high magnification, numerous granular aggregates were clearly observed on the surfaces of the ZFFHI, ZFFHII, and ZFFHIII samples. Additionally, a uniformly dense layer of PDA film was distinctly visible adhering to the surfaces of these samples. It should be noted that there was no significant difference in the surface micromorphology of ZFFHI, ZFFHII, and ZFFHIII samples. This was mainly due to the fact that the different grafting amounts of hyaluronic acid on the ZFFHI, ZFFHII, and ZFFHIII samples did not cause significant micromorphology changes.

The XPS survey spectra of ZE21B, ZF, ZFFHI, ZFFHII, and ZFFHIII samples were shown in Figure 1b, and the corresponding surface chemical compositions were summarized in Table S1. As shown in Figure 1b, Mg, C, O, F, S, and N elements were the six main elements on the sample surfaces. For the ZE21B sample, the three primary elements detected on the surface were Mg, C, and O. The presence of oxygen was likely attributed to metal oxides of magnesium, while the carbon may result from external contamination. After fluoridation, the emerging F 1s photoelectronic peak at 685.4 eV could be clearly observed in the spectrum of ZF sample, caused by the formation of MgF_2 layer on the ZE21B alloy. After the immobilization of fucoidan and hyaluronic acid, the new S 2p and N 1s photoelectronic peaks at 175.0 eV and 400.0 eV appeared in the spectra of ZFFHI, ZFFHII, and ZFFHIII samples because of the sulfur element in the fucoidan and nitrogen element in the hyaluronic acid. As listed in Table S1, the relative atomic contents of the sulfur element on the ZFFHI, ZFFHII, and ZFFHIII samples were 0.53%, 0.40%, and 0.33%, respectively, which exhibited a gradual decrease with the increasing content of hyaluronic acid on the sample surfaces. Moreover, the C/N molar ratios of ZFFHI, ZFFHII, and ZFFHIII samples also presented an increasing tendency along with the

 doi:10.20944/preprints202505.0925.v1

increase of hyaluronic acid on the sample surfaces. The XPS results proved the successful immobilization of fucoidan and hyaluronic acid onto the ZE21B magnesium alloy.

The ATR-FTIR spectra of ZE21B, ZF, ZFFHI, ZFFHII, and ZFFHIII samples were shown in Figure 1c. The spectra of the ZE21B and ZF samples did not exhibit any visible infrared characteristic absorption peaks, which can be attributed to the absence of organic compounds on their surfaces. For fucoidan and hyaluronic acid modified samples, some obvious characteristic adsorption peaks could be observed due to the introduction of organic natural polymer compounds. The broad and strong adsorption peaks at 3343 cm^{-1} could be attributed to the stretching vibration of O-H and N-H bonds in the molecules of fucoidan and hyaluronic acid. The sharp and strong characteristic peak at 1673 cm^{-1} resulted from the stretching vibration of C=O bonds in the amide groups of hyaluronic acid, and the relevant adsorption peak of the stretching vibration of C-N bonds occurred at 1483 cm^{-1}. The strong characteristic adsorption peak at 1132 cm^{-1} was mainly caused by the stretching vibration of S=O and C-O bonds in the sulfonic acid groups, carboxylic acid groups, and amide groups in the fucoidan and hyaluronic acid. The alteration of chemical functional groups on the surface of the samples effectively demonstrated the successful modification of fucoidan and hyaluronic acid onto ZE21B magnesium alloy.

The wettability of material surfaces significantly affects cell adhesion and growth by modulating cell-interface interactions. Moderately hydrophilic surfaces can facilitate initial cell adhesion and spreading [25,26]. The water contact angles of ZE21B, ZF, ZFFHI, ZFFHII, and ZFFHIII samples were shown in Figure 1d. The ZF sample showed the best surface wettability, with the lowest water contact angle of 27.0 ± 1.4º. The water contact angles of ZFFHI, ZFFHII, and ZFFHIII samples were 35.6 ± 1.9º, 36.9 ± 4.5º, and 31.0 ± 0.7º, respectively, which were slightly higher than that of ZF sample and displayed moderate surface wettability. This was mainly because both fucoidan and hyaluronic acid were hydrophilic polymers. Notably, there was no statistical differences in the surface wettability of ZFFHI, ZFFHII, and ZFFHIII samples, suggesting that the different contents of hyaluronic acid did not induce the distinct change of surface hydrophilicity.

The polarization curves of ZE21B, ZF, ZFFHI, ZFFHII, and ZFFHIII samples were shown in Figure 1e, and the corresponding corrosion potentials and corrosion current densities were listed in Table S2. The corrosion resistance of magnesium alloys is crucial to their use as vascular scaffolds. Poor corrosion resistance in magnesium alloy stents can lead to rapid degradation in physiological environments, resulting in premature loss of mechanical support and compromised vascular patency. Conversely, stents that exhibit good corrosion resistance will degrade more slowly and be gradually absorbed by the body after fulfilling their role in vascular remodeling. In general, the lower the corrosion current, the better the corrosion resistance. The ZF sample presented the best corrosion resistance with the corrosion current density of 1.8×10^{-8} A/cm^2, much lower than that of ZE21B sample (1.1×10^{-6} A/cm^2). The corrosion current densities of ZFFHI, ZFFHII, and ZFFHIII samples were 7.8×10^{-7} A/cm^2, 9.6×10^{-7} A/cm^2, and 7.5×10^{-7} A/cm^2, respectively, showing the better corrosion resistance than ZE21B alloy. This was mainly because the MgF_2 layer, PDA layer, fucoidan, and hyaluronic acid served as a physical barrier could collectively protect the ZE21B alloy from rapid corrosion in the corrosive medium.

 doi:10.20944/preprints202505.0925.v1

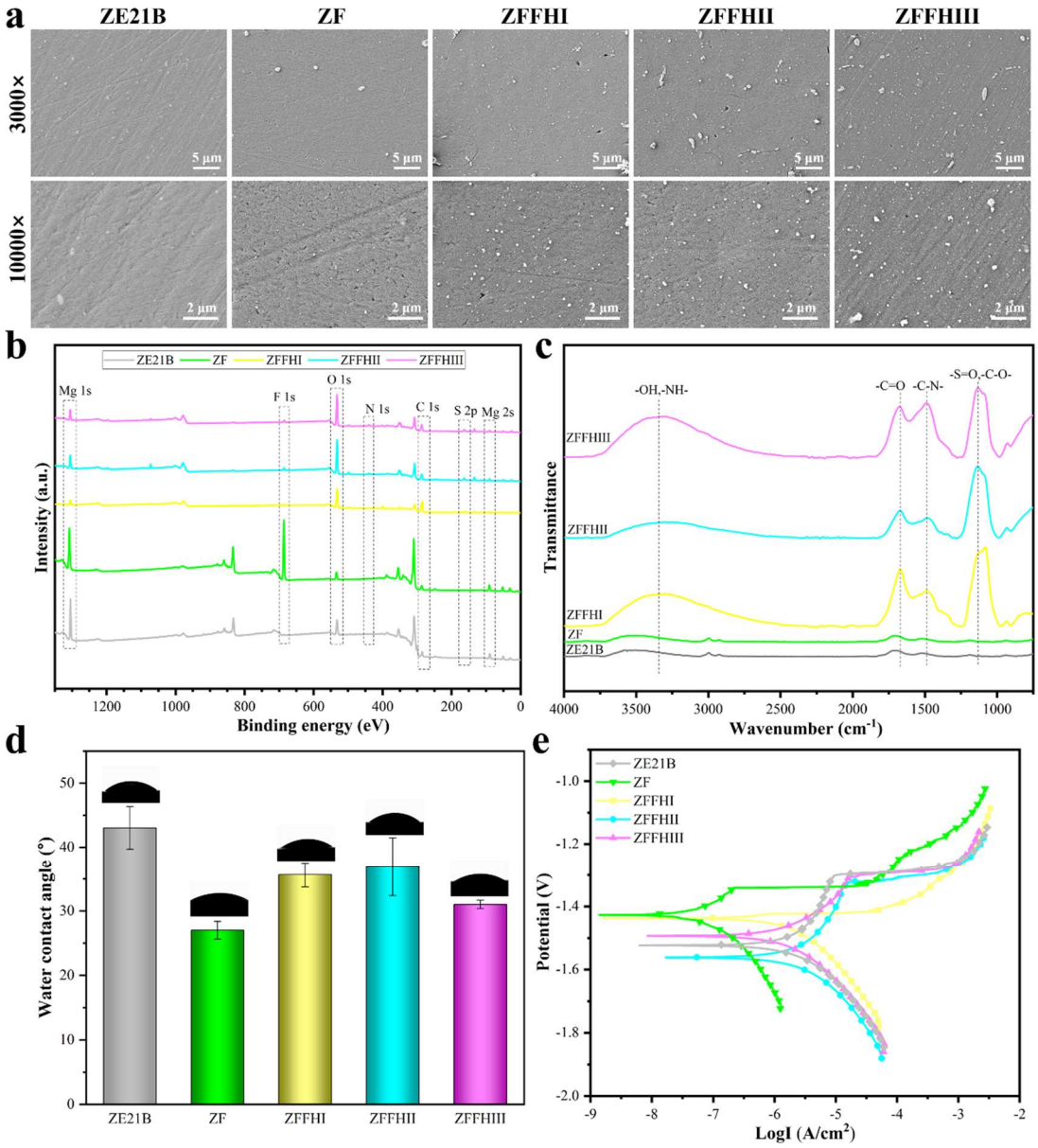

Figure 1. (a) SEM images, (b) XPS survey spectra, (c) ATR-FTIR spectra, (d) water contact angles, and (e) polarization curves of ZE21B, ZF, ZFFHI, ZFFHII, and ZFFHIII samples. (Data were expressed as mean ± SD.).

3.2. In Vitro Hemocompatibility of Fucoidan and Hyaluronic Acid Modified ZE21B Alloy

Hemocompatibility is a critical indicator of the safety and efficacy of blood-contact medical devices, significantly influencing both the clinical risks associated with the device and patient prognosis [27,28]. Direct contact between medical devices and blood can precipitate serious adverse reactions if the surface properties or chemical composition of the materials are not compatible with blood components. Specifically, vascular stents with inadequate blood compatibility are at a heightened risk for thrombus formation on their surfaces, which can result in vessel occlusion or heart failure. Hemolysis assay and fibrinogen adsorption assay were conducted to evaluate the hemocompatibility of ZE21B, ZF, ZFFHI, ZFFHII, and ZFFHIII samples, and the corresponding results were shown in Figure 2. As shown in Figure 2a, the blank ZE21B sample exhibited the highest hemolysis rate at 4.6 ± 0.4%, caused by the release of substantial quantities of metal ions and alterations in the local microenvironmental pH value. The formation of an MgF_2 layer led to a reduction in the hemolysis rate of the ZE21B alloy to 3.8 ± 0.2%. This decrease could be attributed to the protective effect of the MgF_2 layer, which minimized the leaching of metal ions. The hemolysis

 doi:10.20944/preprints202505.0925.v1

rates of ZFFHI, ZFFHII, and ZFFHIII samples were 2.9 ± 0.3%, 2.3 ± 0.5%, and 1.6 ± 0.4%, respectively, much lower than those of ZE21B and ZF samples. This could be primarily attributed to the excellent compatibility of natural fucoidan and hyaluronic acid with red blood cells, which prevents their rupture. Notably, the hemolysis rates of the ZFFHI, ZFFHII, and ZFFHIII samples exhibited a decreasing trend as the concentration of hyaluronic acid on the modified ZE21B alloy increased. This trend suggested a reduction in the risk of hemolysis for the ZE21B magnesium alloy when utilized in vascular stent applications.

Non-specific protein adsorption significantly affects the performances of blood-contact medical devices. The proteins that adsorb onto the device surfaces can modify the material's surface properties, promote platelet adhesion and activation, and contribute to thrombus formation, ultimately leading to vascular occlusion or device malfunction [29,30]. Fibrinogen was selected as a model protein to evaluate the non-specific protein adsorption of ZE21B, ZF, ZFFHI, ZFFHII, and ZFFHIII samples. As shown in Figure 2b, the fibrinogen adsorption levels of ZE21B and ZF samples were much higher than those of ZFFHI, ZFFHII, and ZFFHIII samples. The absence of specific binding sites on the ZE21B and ZF samples hindered the effective repulsion of non-target proteins, resulting in significant adsorption of non-specific proteins. Following modification with natural fucoidan and hyaluronic acid, these two agents demonstrated a synergistic effect in inhibiting non-specific protein adsorption on the ZE21B alloy. In physiological environments, proteins typically exhibit a negative charge; therefore, the negatively charged fucoidan and hyaluronic acid can reduce non-specific protein adsorption by means of electrostatic repulsion. Taking the fibrinogen adsorption level of ZE21B sample as a reference, the fibrinogen adsorption levels of ZFFHI, ZFFHII, and ZFFHIII samples were 0.26, 0.25, and 0.23 times higher than that of ZE21B sample, respectively. The relatively low hemolysis rates (less than 5%) and the minimal fibrinogen adsorption levels observed in the ZFFHI, ZFFHII, and ZFFHIII samples demonstrated the exceptional hemocompatibility of the fucoidan and hyaluronic acid modified ZE21B alloy, making it a suitable candidate for vascular stent applications.

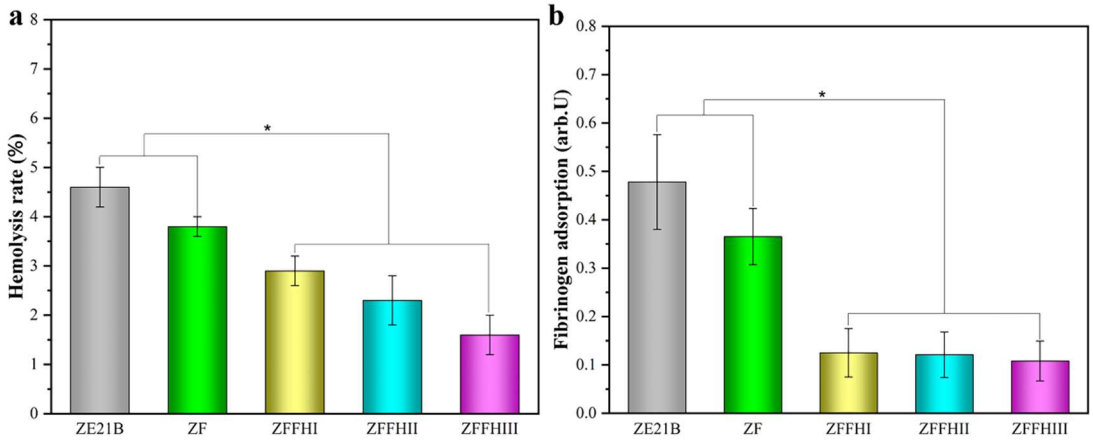

Figure 2. (a) Hemolysis rates and (b) fibrinogen adsorption levels of ZE21B, ZF, ZFFHI, ZFFHII, and ZFFHIII samples. (mean ± SD, *$p < 0.05$ denotes statistically difference between pair.).

3.3. Adhesion, Proliferation, and NO Release of ECs on Modified ZE21B Alloy

The growth behavior of ECs including cell adhesion, cell proliferation, and NO release on the ZE21B, ZF, ZFFHI, ZFFHII, and ZFFHIII samples were investigated through the cell fluorescence staining assays, CCK-8 assays, and NO detection assays. The fluorescence images, proliferation levels, and NO release levels of ECs on the samples after 1 day and 3 days of culture were shown in Figure 3. As illustrated in Figure 3a, the substantial accumulation of metal ions resulting from the degradation of the ZE21B alloy led to apoptosis in the surrounding cells. Consequently, after 1 day and 3 days of cell culture, there were nearly no ECs in a healthy condition on the ZE21B alloy surface.

 doi:10.20944/preprints202505.0925.v1

For ZF, ZFFHI, ZFFHII, and ZFFHIII samples, the ECs on these samples could normally grow, spread and proliferate after 1 day and 3 days of culture. On day 1, the ECs on the samples displayed either rounded or irregular morphologies, accompanied by a limited coverage area. This observation suggested that the cells were in a growth status that had not yet reached full spreading. The number of ECs in the ZFFHI and ZFFHIII groups was significantly higher than that in the other groups. On day 3, the ECs on the ZF, ZFFHI, ZFFHII, and ZFFHIII samples exhibited a flattened polygonal or cobblestone-like morphology. The cells displayed clearly defined margins and abundant pseudopods, indicating effective spreading across the sample surfaces. In addition to a significant increase in the coverage area of ECs, the number of ECs on the samples was also significantly increased, especially for the ZFFHI, ZFFHII, and ZFFHIII groups.

The results of CCK-8 assays and cell fluorescence staining assays were basically consistent. As shown in Figure 3b, after 1 day of cell culture, the ECs on each sample were at a low proliferation level and the ZFFHI group showed the highest level of cell proliferation. After 3 days of cell culture, the proliferation levels of ECs were significantly higher in all experimental groups. The proliferation levels of ECs in ZFFHI, ZFFHII, and ZFFHIII groups were obviously higher than those of ZE21B and ZF groups. Taking the cell proliferation level of ZF group as a reference, the cell proliferation levels of ZFFHI, ZFFHII, and ZFFHIII groups were 2.46, 2.67, and 2.73 times higher than that of ZF group, respectively. In addition, there was no statistically significant difference in the proliferation level of ECs between ZFFHII and ZFFHIII groups. The growth rate of ECs in ZFFHI, ZFFHII, and ZFFHIII groups were distinctly higher than that in ZF group, suggesting the natural fucoidan and hyaluronic acid could promote the rapid proliferation of ECs on the modified ZE21B alloy.

No gas signaling molecule significantly affects ECs and SMCs. It can maintain the normal physiological functions of ECs, promote the release of vasodilatory factors, and preserve endothelial integrity. Additionally, it inhibits the excessive proliferation of SMCs and prevent vascular stenosis [31,32]. The NO release levels of ECs on the ZE21B, ZF, ZFFHI, ZFFHII, and ZFFHIII samples after 1 day and 3 days of culture were shown in Figure 3c. After 1 day of cell culture, the NO release levels of ECs in ZFFHI, ZFFHII, and ZFFHIII groups were obviously higher than those of ECs in ZE21B and ZF groups, though all were at a lower level. After 3 days of cell culture, NO release levels were significantly higher in all experimental groups except for ZE21B group, indicating that these ECs were in a favorable growth microenvironment. The NO release levels of ECs in the ZFFHI, ZFFHII, and ZFFHIII groups were 2.69, 3.10 and 2.37 times higher than that of ECs in the ZF group, respectively. Among the ZFFHI, ZFFHII, and ZFFHIII groups, the ZFFHII groups presented the highest NO release level, suggesting that the optimal composition of fucoidan and hyaluronic acid on the ZE21B alloy could be more favorable for providing a good microenvironment for ECs growth, activating nitric oxide synthase in the ECs, and enhancing cell growth activity.

 doi:10.20944/preprints202505.0925.v1

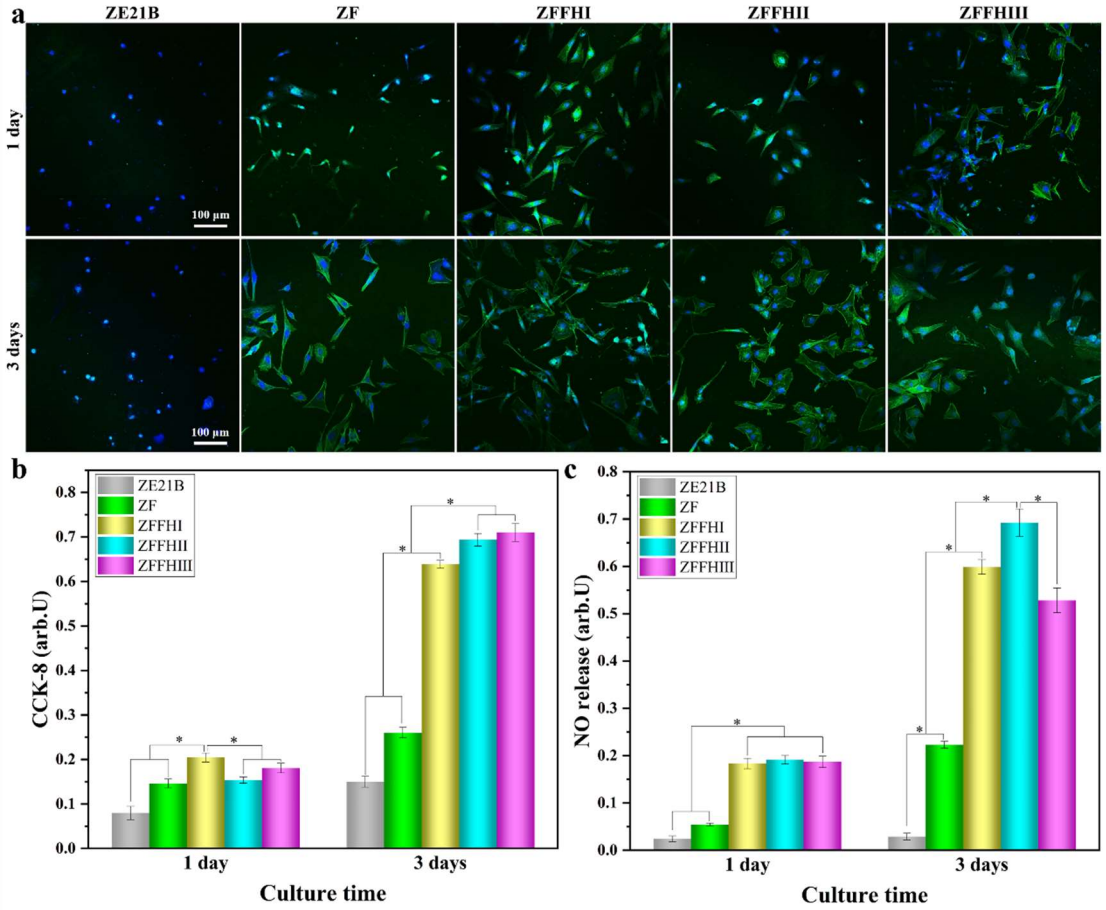

Figure 3. (a) Fluorescence images, (b) proliferation levels (evaluated by CCK-8 assay), and (c) NO release levels of ECs cultured on the ZE21B, ZF, ZFFHI, ZFFHII, and ZFFHIII samples for 1 day and 3 days. (mean ± SD, $*p < 0.05$ denotes statistically difference between pair.).

3.4. Adhesion and Proliferation of SMCs on Modified ZE21B Alloy

Vascular SMCs significantly influence the performance of vascular stents. Following stent implantation, SMCs migrate from the medial layer to the intima and undergo extensive proliferation, with their phenotypic transformation being associated with in-stent restenosis. Excessive proliferation of SMCs can result in neointimal thickening, which narrows the vessel lumen and compromises stent patency [33,34]. The adhesion and proliferation of SMCs on the ZE21B, ZF, ZFFHI, ZFFHII, and ZFFHIII samples after 1 day and 3 days of culture were investigated through the cell fluorescence staining assays and CCK-8 assays, and the corresponding results were shown in Figure 4. The fluorescence images of these SMCs on the samples at the predetermined time points were displayed in Figure 4a. The elevated concentration of metal ions released from the degradation of ZE21B alloy induced apoptosis in SMCs, resulting in a significant reduction of viable SMCs on the ZE21B surface after 1 and 3 days of culture. On day 1, the SMCs exhibited normal adhesion and growth on the ZF, ZFFHI, ZFFHII, and ZFFHIII samples; however, both the coverage area and the quantity of SMCs on these samples remained low. The number of SMCs in ZFFHI, ZFFHII, and ZFFHIII groups was distinctly higher than that in ZF group. After 3 days of cell culture, the spreading area and quantity of SMCs on the ZF, ZFFHI, ZFFHII, and ZFFHIII samples were significantly enhanced. These SMCs exhibited an elongated, shuttle-like shape on the surfaces, displaying distinct cell outlines and maintaining stable morphology.

The proliferation levels of SMCs determined by CCK-8 assays on the samples after 1 day and 3 days of cell culture were shown in Figure 4b. On day 1, the proliferation levels of SMCs in ZFFHI, ZFFHII, and ZFFHIII groups were much higher than those in ZE21B and ZF groups. When the cell

 doi:10.20944/preprints202505.0925.v1

culture time was extended to 3 days, the number of SMCs in the ZF, ZFFHI, ZFFHII, and ZFFHIII groups increased, especially for the ZF group. The ZFFHIII groups exhibited the highest proliferation level of SMCs, and there was no statistical difference in the number of SMCs in ZF, ZFFHI, and ZFFHII groups. In comparison to the ZF group, the proliferation of SMCs in ZFFHI, ZFFHII, and ZFFHIII groups was obviously inhibited to a certain extent, although the number of SMCs increased, which was mainly due to the inhibitory effects of fucoidan and hyaluronic acid on SMCs proliferation.

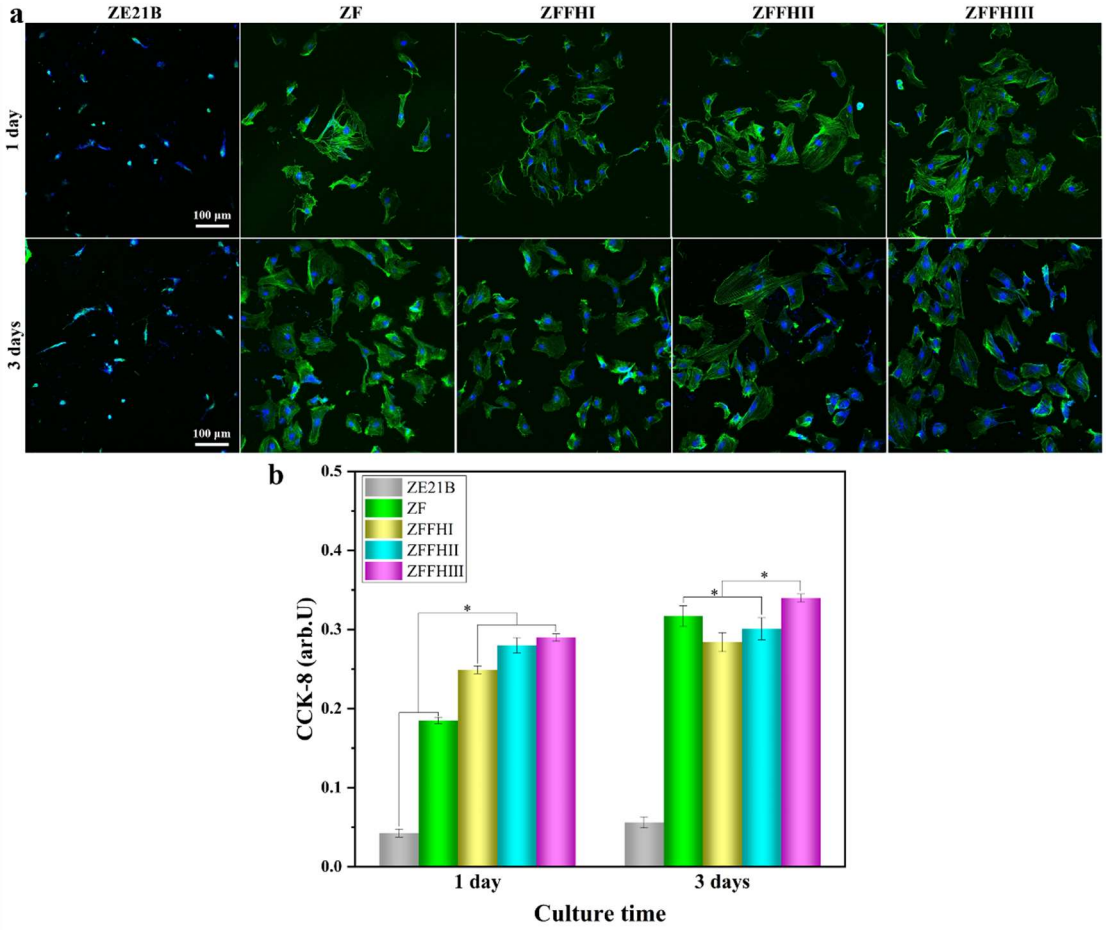

Figure 4. (a) Fluorescence images and (b) proliferation levels (evaluated by CCK-8 assay) of SMCs cultured on the ZE21B, ZF, ZFFHI, ZFFHII, and ZFFHIII samples for 1 day and 3 days. (mean ± SD, *p < 0.05 denotes statistically difference between pair.).

3.5. Competitive Growth of ECs and SMCs on Modified ZE21B Alloy

The competitive growth of SMCs and ECs significantly influences the performance of vascular stents [35,36]. Excessive proliferation of SMCs can lead to their migration to the intima, where they secrete extracellular matrix, resulting in neointimal thickening. This process may trigger in-stent restenosis and compromise vessel patency. Conversely, well-developed ECs can effectively prevent thrombosis by properly covering the stent's surface. When these two cell types compete for growth, a scenario in which ECs are inhibited and SMCs dominate can diminish the stent's anti-thrombotic and anti-restenosis properties. In contrast, if ECs prevail, normal vascular function is upheld, thereby ensuring the long-term efficacy of the stent. The competitive growth behavior of ECs and SMCs on the ZE21B, ZF, ZFFHI, ZFFHII, and ZFFHIII samples after 1 day of coculture were evaluated through cell fluorescence staining assays in the same culture system. The fluorescence images of ECs stained with green and SMCs stained with red on the samples were shown in Figure 5a, and the corresponding cell densities and ratios of ECs/SMCs were presented in Figure 5b. The ECs and SMCs

 doi:10.20944/preprints202505.0925.v1

in the ZE21B, ZF, ZFFHI, ZFFHII, and ZFFHIII groups could normally grow and proliferate after 1 day of culture. The total number of ECs and SMCs in the ZFFHI, ZFFHII, and ZFFHIII groups was significantly higher than that in the ZE21B and ZF groups. For instance, the cell densities of ECs and SMCs in the ZF group were observed to be 75.0 ± 2.4 cells/mm² and 47.5 ± 2.3 cells/mm², respectively. In contrast, the ZFFHII group exhibited significantly higher cell densities of 212.5 ± 3.1 cells/mm² for ECs and 115.0 ± 2.4 cells/mm² for SMCs. The ratios of ECs/SMCs in ZFFHI, ZFFHII, and ZFFHIII groups were 1.75, 1.85, and 1.56, respectively. The ZFFHII group possessed the highest ratio of ECs/SMCs, which revealed that an appropriate composition of fucoidan and hyaluronic acid on the ZE21B alloy could significantly enhance the competitive growth advantage of ECs over SMCs. The growth advantage of ECs over SMCs on the fucoidan and hyaluronic acid modified ZE21B alloy had the potential in facilitating the rapid endothelialization and inhibiting intimal hyperplasia.

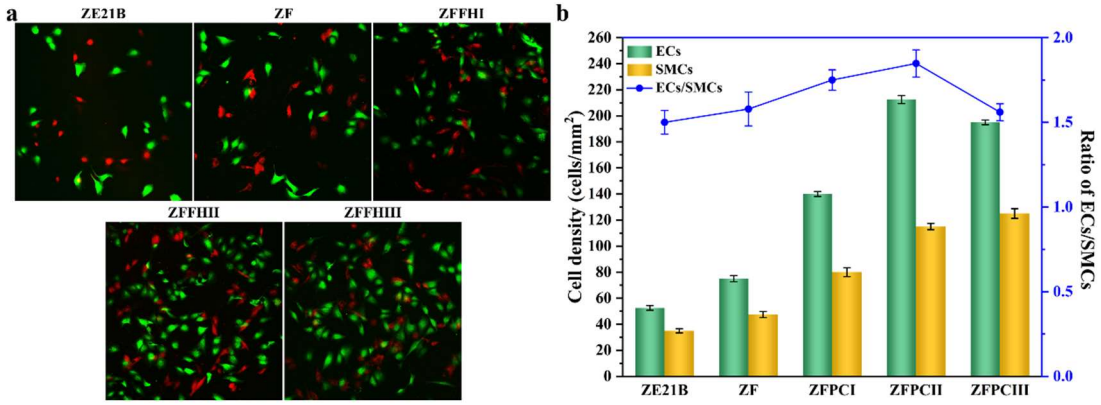

Figure 5. (a) Fluorescence images of ECs and SMCs on ZE21B, ZF, ZFFHI, ZFFHII, and ZFFHIII samples after co-culture for 1 day, (b) corresponding cell densities and ratios of ECs/SMCs on different sample surfaces at day 1. (mean ± SD, *$p < 0.05$ denotes statistically difference between pair.).

4. Conclusions

In summary, we developed a composite coating consisting of MgF_2 layer, PDA layer, fucoidan, and hyaluronic acid to enhance corrosion resistance and biocompatibility ZE21B alloy for vascular stent application. The MgF_2 layer and PDA layer in the composite coating can collectively protect ZE21B alloy from too fast degradation. The composite coating modified ZE21B alloy with lower corrosion current density showed better corrosion resistance in comparison to bare ZE21B alloy. The natural fucoidan and hyaluronic acid in the coating could significantly improve the hemocompatibility of ZE21B alloy and regulate the cellular behavior of vascular cells on the ZE21B alloy. The modified ZE21B alloy could promote the adhesion, proliferation, and NO release of ECs and enhance the competitive growth advantage of ECs over SMCs. This work provided a simple and effective strategy for the development of biomacromolecule-based functional coatings for the application of biodegradable vascular stents.

Supplementary Materials: The following supporting information can be downloaded at the website of this paper posted on Preprints.org, Table S1. Surface chemical compositions (At.%) of ZE21B, ZF, ZFFHI, ZFFHII and ZFFHIII samples de-termined by XPSTable S2. Corrosion potentials (Ecorr) and corrosion current densities (Icorr) of ZE21B, ZF, ZFFHI, ZFFHII and ZFFHIII samples in Hanks' solution determined by the electrochemical method..

Author Contributions: Conceptualization, L.C. Bai and S.K. Guan; methodology, H.R. Wang and Y.W. Gu; investigation, H.R. Wang and Y.W. Gu; data curation, H.R. Wang and Q. Wang; Resources, L.C. Bai and S.K. Guan; Writ-ing—original draft preparation, H.R. Wang; Writing—review and editing, L.C. Bai and S.K. Guan. All au-thors have read and agreed to the published version of the manuscript.

 doi:10.20944/preprints202505.0925.v1

Funding: This work was supported by the Scientific and Technological Project in Henan Province (Grant No. 242102231056), China Postdoctoral Science Foundation (Grant No. 2024M762987).

Institutional Review Board Statement: Not applicable.

Informed Consent Statement: Not applicable.

Data Availability Statement: Data is contained within the article.

Conflicts of Interest: The authors declare no conflicts of interest.

References

1. Khan S.Q.; Ludman P.F. Percutaneous coronary intervention. *Medicine* **2022**, *50*, 437-444.
2. Im S.H.; Im D.H.; Park S.J.; Jung Y.; Kim D.H.; Kim S.H. Current status and future direction of metallic and polymeric materials for advanced vascular stents. *Prog. Mater. Sci.* **2022**, *126*, 100922.
3. Guan S.; Mei D.; Wang J.; Zhang Z.Q.; Du P.H.; Bai L.C.; Yan C.; Li J.A.; Wang J.; Zhu S.J. Mg alloy cardio-/cerebrovascular scaffolds: Developments and prospects. *J. Magnes. Alloys* **2023**, *11*, 4011-4042.
4. Bai L.C.; Wang Y.H.; Chen L.; Wang J.; Li J.A.; Zhu S.J.; Wang L.G.; Guan S.K. Preparation of functional coating on magnesium alloy with hydrophilic polymers and bioactive peptides for improved corrosion resistance and biocompatibility. *J. Magnes. Alloys* **2022**, *10*, 1957-1971.
5. Zhang Z.Q.; Yang Y.X.; Li J.A.; Zeng R.C.; Guan S.K. Advances in coatings on magnesium alloys for cardiovascular stents–a review. *Bioact. Mater.* **2021**, *6*, 4729-4757.
6. Wang Y.H.; Chen L.; Hou R.Q.; Bai L.C.; Guan S.K. Rapamycin-loaded nanocoating to specially modulate smooth muscle cells on ZE21B alloy for vascular stent application. *Appl. Surf. Sci.* **2023**, *615*, 156410.
7. Bai L.C.; Wang Y.H.; Xie J.; Zhao Y.; Guan S.K. Fucoidan-based coating on magnesium alloy improves the hemocompatibility and pro-endothelialization potential for vascular stent application. *Mater. Des.* **2023**, *233*, 112235.
8. Imandoust A.; Barrett C.D.; Al-Samman T.; Inal K.A.; El Kadiri H. A review on the effect of rare-earth elements on texture evolution during processing of magnesium alloys. *J. Mater. Sci.* **2017**, *52*, 1-29.
9. Yao W.; Tan Y.; Lu Q.; Yi H.; Cheng C.; Wu L.; Saji V.S.; Pan F. Recent advances in protective coatings and surface modifications for corrosion protection of Mg alloys. *J. Mater. Res. Technol.* **2024**, *31*, 3238-3254.
10. Wang Y.H.; Zhao Y.; Wang X.Y.; Xie Y.D.; Bai L.C.; Guan S.K. Fucoidan/collagen composite coating on magnesium alloy for better corrosion resistance and pro-endothelialization potential. *Int. J. Biol. Macromol.* **2024**, *255*, 128044.
11. Yao W.; Wu L.; Wang J.; Jiang B.; Zhang D.; Serdechnova M.; Shulha T.; Blawert C.; Zheludkevich M.L.; Pan F. Micro-arc oxidation of magnesium alloys: A review. *J. Mater. Sci. Technol.* **2022**, *118*, 158-180.
12. Zhao Y.; Wang Y.; Chen L.; Bai L.C.; Guan S.K. Co-immobilization of natural marine polysaccharides and bioactive peptides on ZE21B magnesium alloy to enhance hemocompatibility and cytocompatibility. *Int. J. Biol. Macromol.* **2024**, *272*, 132747.
13. Wang X.; Zhao Y.; Gu Y.; Bai L.; Chen L.; Guan S. Chondroitin sulfate and Cys-Ala-Gly peptides coated ZE21B magnesium alloy for enhanced corrosion resistance and vascular compatibility. *Int. J. Biol. Macromol.* **2025**, *311*, 143895.
14. Zhang H.D., Chen A.Y., Gan B.; Jiang H.; Gu L.J. Corrosion protection investigations of carbon dots and polydopamine composite coating on magnesium alloy. *J. Magnes. Alloys* **2022**, *10*, 1358-1367.
15. Liu X.; Zhen Z.; Liu J.; Xi T.; Zheng Y.; Guan S.; Zheng Y.; Cheng Y. Multifunctional MgF_2/polydopamine coating on Mg alloy for vascular stent application. *J. Mater. Sci. Technol.* **2015**, *31*, 733-743.
16. Hu S.; Du H.; Huang H.; Wei Y.; Hou L.; Wang Q.; Wei H.; Liu X.; Zhou Y.; He H.W. Deposition of modifiable MAO-PDA coatings on magnesium alloy based on photocatalytic effect. *Appl. Surf. Sci.* **2024**, *669*, 160522.
17. Venkatesan J.; Murugan S.S.; Seong G.H. Fucoidan-based nanoparticles: Preparations and applications. *Int. J. Biol. Macromol.* **2022**, *217*, 652-667.
18. Yao Y.; Zaw A.M.; Anderson D.E.J.; Hinds M.T.; Yim E.Y.K. Fucoidan functionalization on poly (vinyl alcohol) hydrogels for improved endothelialization and hemocompatibility. *Biomaterials* **2020**, *249*, 120011.
19. Marinval N.; Morenc M.; Labour M.N.; Samotus A.; Mzyk A.; Ollivier V.; Maire M.; Jesse K.; Bassand K.; Niemiec-Cyganek A.; Haddad O.; Jacob M.P.; Chaubet F.; Charnaux N.; Wilczek P.; Hlawaty H.

 doi:10.20944/preprints202505.0925.v1

Fucoidan/VEGF-based surface modification of decellularized pulmonary heart valve improves the antithrombotic and re-endothelialization potential of bioprostheses. *Biomaterials* **2018**, *172*, 14-29.
20. Simińska-Stanny J.; Podstawczyk D.; Delporte C.; Nie L.; Shavandi A. Hyaluronic acid role in biomaterials prevascularization. *Adv. Healthcare Mater.* **2024**, *13*, 2402045.
21. Zhao Y.; Li M.; Chen N.; Huang K.; Wu X.; Tan Y.; Hu Q.; Luo R.; Wang Y. Multifunctional hyaluronic acid-based coating to direct vascular cell fate for enhanced vascular tissue healing. *Int. J. Biol. Macromol.* **2025**, *288*, 138741.
22. Jia W.; Liu L.; Li M.; Zhou Y.; Zhou H.; Weng H.; Gu G.; Xiao M.; Chen Z. Construction of enzyme-laden vascular scaffolds based on hyaluronic acid oligosaccharides-modified collagen nanofibers for antithrombosis and in-situ endothelialization of tissue-engineered blood vessels. *Acta Biomater.* **2022**, *153*, 287-298.
23. Lu D.; Cai K.; Zeng Z.; Huang J.; Ma N.; Gao B.; Yu S. VEGF loading heparinized hyaluronic acid macroporous hydrogels for enhanced 3D endothelial cell migration and vascularization. *Biomater. Adv.* **2025**, *167*, 214094.
24. Feng L.A.; Shi J.; Guo J.Y.; Wang S.F. Recent strategies for improving hemocompatibility and endothelialization of cardiovascular devices and inhibition of intimal hyperplasia. *J. Mater. Chem. B* **2022**, *10*, 3781-3792.
25. Amani H.; Arzaghi H.; Bayandori M.; Shiralizadeh A.; Pazoki-Toroudi H.; Shafiee A.; Moradi L. Controlling cell behavior through the design of biomaterial surfaces: a focus on surface modification techniques. *Adv. Mater. Interfaces* **2019**, *6*, 1900572.
26. Nascimento A.T.; Mendes A.X.; Duchi S.; Duc D.; Aguilar L.C.; Quigley A.F.; Kapsa B.M.I.; Nisbet D.R.; Stoddart P.R.; Silva S.M.; Moulton S.E. Wired for success: Probing the effect of tissue-engineered neural interface substrates on cell viability. *ACS Biomater. Sci. Eng.* **2024**, 10, 3775-3791.
27. Roberts T.R.; Garren M.R.S.; Wilson S.N.; Handa H.; Batchinsky A.I. Development and in vitro whole blood hemocompatibility screening of endothelium-mimetic multifunctional coatings. *ACS Appl. Bio Mater.* **2022**, *5*, 2212-2223.
28. Nazari S.; Abdelrasoul A. Impact of membrane modification and surface immobilization techniques on the hemocompatibility of hemodialysis membranes: A critical review. *Membranes* **2022**, *12*, 1063.
29. Luu C.H.; Nguyen N.T.; Ta H.T. Unravelling surface modification strategies for preventing medical device-induced thrombosis. *Adv. Healthcare Mater.* **2024**, *13*, 2301039.
30. Kuchinka J.; Willems C.; Telyshev D.V.; Groth T. Control of blood coagulation by hemocompatible material surfaces—a review. *Bioengineering* **2021**, *8*, 215.
31. Gao Y.; Bai S.; Zhu K.; Yuan X. Electrospun membranes of diselenide-containing poly (ester urethane) urea for in situ catalytic generation of nitric oxide. *J. Biomater. Sci.* **2024**, *35*, 1157-1176.
32. Zeng Z.; Liu T.; Zeng P.; Xie Y.; Li L.; Tan J.; Wang H.; Liu S.; Bian Q.; Xiao H.; Liang S.; Chen J.; Chen Y.; Lu L. Enhancing vascular implants with heparin-polylysine-copper nanozyme coating for synergistic anticoagulation and antirestenotic activity. *Int. J. Biol. Macromol.* **2025**, *309*, 143048.
33. Kang M.K.; Heo S.H.; Yoon J.K. In-stent re-endothelialization strategies: Cells, extracellular matrix, and extracellular vesicles. *Tissue Eng. Part B*, **2024**.
34. Wu M.; Xun M.; Chen Y. Adaptation of vascular smooth muscle cell to degradable metal stent implantation. *ACS Biomater. Sci. Eng.* **2023**, *9*, 4086-4100.
35. Qiu H.; Qi P.; Liu J.; Yang Y.; Tan X.; Xiao Y.; Maitz M.F.; Huang N.; Yang Z. Biomimetic engineering endothelium-like coating on cardiovascular stent through heparin and nitric oxide-generating compound synergistic modification strategy. *Biomaterials*, **2019**, *207*, 10-22.
36. Zhao J., Feng Y. Surface engineering of cardiovascular devices for improved hemocompatibility and rapid endothelialization. *Adv. Healthcare Mater.* **2020**, *9*, 2000920.